

PCCP

Accepted Manuscript

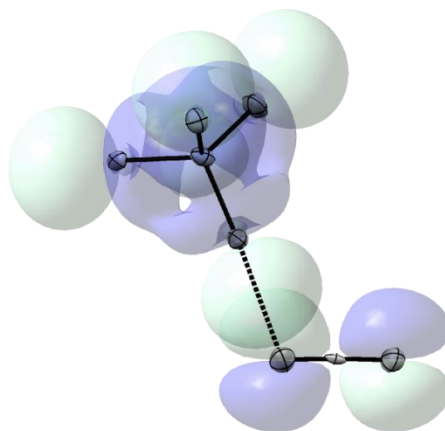


This is an *Accepted Manuscript*, which has been through the Royal Society of Chemistry peer review process and has been accepted for publication.

Accepted Manuscripts are published online shortly after acceptance, before technical editing, formatting and proof reading. Using this free service, authors can make their results available to the community, in citable form, before we publish the edited article. We will replace this *Accepted Manuscript* with the edited and formatted *Advance Article* as soon as it is available.

You can find more information about *Accepted Manuscripts* in the [Information for Authors](#).

Please note that technical editing may introduce minor changes to the text and/or graphics, which may alter content. The journal's standard [Terms & Conditions](#) and the [Ethical guidelines](#) still apply. In no event shall the Royal Society of Chemistry be held responsible for any errors or omissions in this *Accepted Manuscript* or any consequences arising from the use of any information it contains.

Halogen bonding of electrophilic bromocarbons with pseudohalide anions[‡]Sergiy V. Rosokha,^{†,*} Charlotte L. Stern,[§] Alan Swartz[†] and Rory Stewart[†]

Spectral, thermodynamic and structural features of the complexes of bromocarbons with polydentate azide, cyanate or thiocyanate anions are presented. They suggest significant role of the molecular-orbital interactions in formation of these halogen-bonded associates

[†] Department of Biological, Chemical and Physical Sciences
Roosevelt University, Chicago, IL, 60605, USA
E-mail: srosokha@roosevelt.edu

[§] Department of Chemistry, Northwestern University, Evanston, Illinois 60208

[‡] Electronic Supplementary Information (ESI) available: Details of experimental UV-Vis and FT-IR measurements and quantum-mechanical computations. See DOI: 10.1039/c000000x/

Abstract

UV-Vis measurements showed that the interaction of pseudohalide anions, A^- ($A^- = N_3^-$, NCO^- , NCS^-) with electrophilic bromocarbons, R-Br (R-Br = CBR_4 , CBR_3NO_2 , CBR_3CONH_2 , CBR_3H , CBR_3F , CBR_3CN or $C_3Br_2F_6$) in solution results in formation of [R-Br, A^-] complexes. These associates are characterized by intense absorption bands in the 200 - 350 nm range showing distinct Mulliken correlation with the frontier (HOMO/LUMO) orbitals' separations of the interacting anion and R-Br electrophile. X-ray crystallographic studies established the principal structural features of the halogen-bonded associates between bromocarbons and polydentate pseudohalide anions. Specifically, in the $(Pr_4N)NCO \cdot CBR_4$, $(Pr_4N)N_3 \cdot CBR_4$ and $(Pr_4N)NCO \cdot CBR_3NO_2$ co-crystals, bromine substituents of the electrophiles are halogen-bonded with the ($C \equiv N$ or $N = N$) π -bonds of the cyanate or azide anions. Co-crystals of CBR_4 with $(Pr_4N)NCS$ show two modes ($C-Br \dots S-C$ and $C-Br \dots N \equiv C$) of halogen bonding, while tribromoacetamide molecules form $C-Br \dots S-C$ halogen bonds and $N-H \dots N \equiv C$ hydrogen bonds with thiocyanate anions. Structures and energetics of the halogen-bonded complexes resulted from the M06-2X/6-311+G(dp) computations of various R-Br/ A^- pairs were consistent with the experimental data. These computations revealed that the variations of the intramolecular (C-Br) and intermolecular (Br... A^-) bond lengths are correlated with the $A^- \rightarrow$ R-Br charge transfer determined from Natural Bond Orbital analysis. Also, scrutiny of the structural data indicated that the locations of the intermolecular contacts in these associates are determined primarily by the frontier orbital shapes of the halogen-bonded species. Thus, spectral and structural data point out a significant role of molecular-orbital (charge-transfer) interactions in formation of halogen bonded complexes involving pseudohalides and bromocarbons.

Introduction

Intermolecular interactions involving electrophilic halogen atoms, referred to as halogen bonding, emerged during the last decade as a topical area of supramolecular chemistry.[1-3] Electron-rich anions represent a prototypical halogen-bond acceptor, and several recent publications demonstrated that their interaction with halogenated molecules may be used for molecular recognition and transport of anionic species,[4,5] as well as for crystal engineering of hybrid materials combining neutral organic molecules and ionic salts.[6,7] Up to now, however, the studies on halogen bonding with anions were focused primarily on the structural characterization of the solid-state networks formed by halogenated electrophiles with halide and halometallate salts, and, to a lesser extent, on the evaluation of the thermodynamics of halogen bonded complexes involving halide anions in solutions.[5-11] In addition, there are several examples of the solid-state studies of halogen bonding with polyoxoanions, metallocyanides and other anionic species.[12-14]

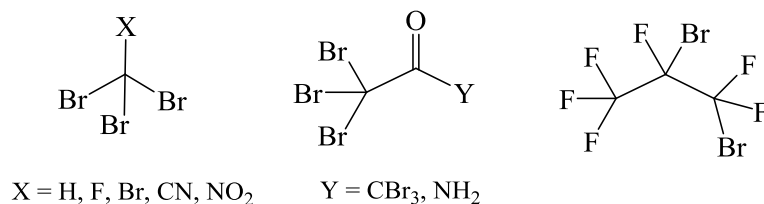
In contrast to halides, studies of halogen bonding involving pseudohalides are limited mostly to characterization of several solid-state associates of iodo- and bromosubstituted organic molecules with thiocyanate anion and its metal complexes.[11,15-17] In fact, the CCSD database search did not return any examples of short intermolecular contact between covalently-bound halogen and separate azide or cyanate anions.[18] Such omission is surprising, since NCS^- , NCO^- and N_3^- anions play a major role in various areas of chemistry and biochemistry, and represent effective building blocks in crystal engineering and material science.[19-22] For example, the “flexidentate” nature and bridging capacities of azide anions as regards to metal-ion coordination facilitated preparation of a variety of magnetic substances, catalysts of photochemical processes

and high energy density materials.[20] The NCS^- and N_3^- anions have been frequently used as crystallizing agents in protein crystallography and are known to be competitive inhibitors in many enzymes (e.g. superoxide dismutase, carbonic anhydrase, etc.). [20] As such, characterization of halogen-bonded complexes with participation of pseudohalides may add halogen bonding as a valuable tool for preparation of hybrid molecular materials combining advantageous features of organic and inorganic molecules. It may also facilitate clarification of the possible involvement of this interaction in biochemical systems.

Interest to the complexes with NCO^- , NCS^- and N_3^- anions is related also to the fact that the pseudohalides have been employed extensively as probes in the study of intermolecular interactions (e.g. ionic association, hydrogen bonding) in solution and in solid state.[22,23] Indeed, while halides are spherically-symmetrical species, the study of halogen-bonded complexes of pseudohalide anions allows an examination of the factors which determine the location and geometry of halogen bonds at the halogen-bond acceptor side. The polydentate nature of pseudohalide anions, which is well-known in metal-ion coordination chemistry and was demonstrated earlier in the halogen-bonded associates of thiocyanate with iodosubstituted molecules[16] facilitates comparison of several potential modes of bonding, such as $\text{C-X} \dots \text{O}$ and $\text{C-X} \dots \text{N}$ interaction (where X is a halogen atom), $\text{C-X} \dots \text{lone-pair}$ vs $\text{C-X} \dots \pi$ -bond interactions, etc. Besides, NCS^- , NCO^- and N_3^- anions are relatively small species with two bonds. As such, the effects of halogen bonding on their structural and spectral features should be more pronounced than in large anionic species (e.g. halometallates or polyoxoanions).

Accordingly, in the current work, we present the results of experimental and computational studies of intermolecular interactions between the bromocarbons illustrated in Chart 1 and pseudohalide (NCS^- , NCO^- , N_3^-) anions.

Chart 1. Halogen Bond (XB) Donors R-Br.



In particular, the solution-phase UV-Vis measurements establish spectral and thermodynamic properties of these complexes. The X-ray crystallographic characterization of the solid-state associates provides structural characteristics of the halogen bonding with participation of these polydentate anions and reveals the effects of the intermolecular interactions on the interacting species. Together with the computational analysis of the separate components and their adducts, the experimental characteristics of the halogen-bonded complexes presented herein provide further insight into the nature and properties of halogen bonding, which may be helpful for crystal engineering involving pseudohalide anions, as well as for molecular recognition and transport of these species in chemical and biochemical systems.

Results and Discussion.

1. UV-Vis spectroscopic study of the interaction between bromocarbons and anions.

Similar to the earlier reported systems with the halide anions,[9, 10, 15] UV-Vis spectra of dichloromethane solutions containing pseudohalide anions together with the R-Br electrophiles show absorption bands in the 200 – 350 nm range, which are not present in the spectra of the separate components. For example, addition of $(\text{Bu}_4\text{N})\text{NCS}$ salt to the solution of fluorotri-bromomethane resulted in the instantaneous appearance of a new absorption band at 289 nm (Figure 1). The intensity of this band grew with increasing concentration of thiocyanate at constant concentration of CBr_3F (or vice versa), and with lowering the temperature of the solution at constant concentrations of the reagents. [Note, that variations of concentration of the Bu_4N^+ counter-ion did not affect UV-Vis spectra, and essentially the same results were obtained with tetrapropylammonium salts.]

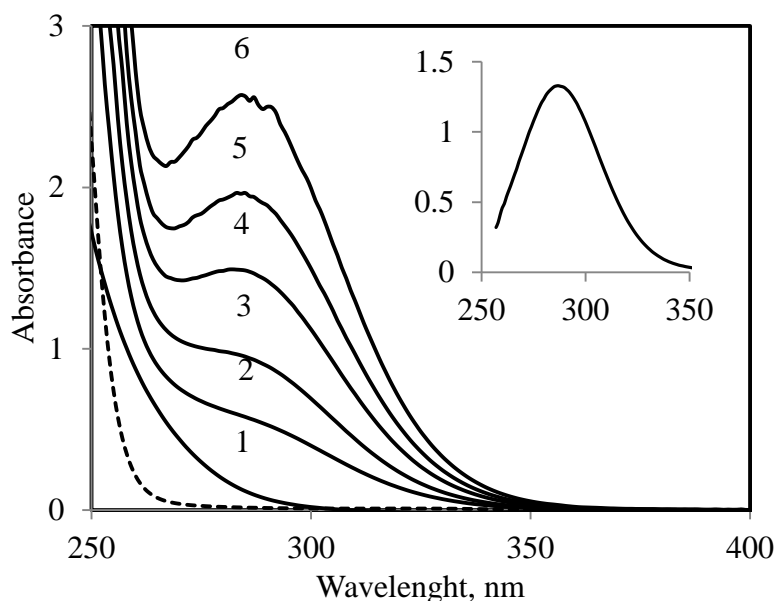


Figure 1. Spectral changes resulting from the addition of $(\text{Bu}_4\text{N})\text{NCS}$ to 4.7 mM solution of CBr_3F in dichloromethane (19 °C). Concentration of $(\text{Bu}_4\text{N})\text{NCS}$ (solid lines): 0 mM (1), 40 mM (2), 82 mM (3), 144 mM (4), 188 mM (5), and 252 mM (6). Dashed line corresponds to the separate 40 mM solution of $(\text{Bu}_4\text{N})\text{NCS}$. Inset: Absorption band of $[\text{CBr}_3\text{F}, \text{NCS}]$ complex which was obtained by subtraction of the absorption of $(\text{Bu}_4\text{N})\text{NCS}$ and CBr_3F reagents from the spectrum (4) of their mixture.

New absorption bands which appeared in the solutions containing one of the R-Br electrophiles and one of the pseudohalide anions showed, in most cases, similar behavior (see Experimental Section and Figures S1 - S5 in the Supporting Information). Analysis of the dependencies of intensities of these new bands (obtained, in general, by subtraction of the absorption of components from the absorption of their mixture) on the concentration of components according to the Job's method indicated that they are related in most cases to reversible formation of 1:1 complexes (see Experimental Section for details):



The absorption band maxima for the $[\text{R-Br}, \text{A}^-]$ complexes and the equilibrium constants of their formation resulted from spectral measurements are summarized in Table 1.

Table 1. Absorption band maxima and formation constants of $[\text{R-Br}, \text{A}^-]$ complexes.^a

R-Br	N_3^-		NCS^-		NCO^-	
	λ_{max} , nm	K, M^{-1}	λ_{max} , nm	K, M^{-1}	λ_{max} , nm	K, M^{-1}
CBr_3NO_2	303, 360 ^b	$\sim 6^b$	284, 330 ^b	- ^b	251, 297	5
CBr_3CN	315 ^b	- ^b	300 ^b	$\sim 1.6^b$	265	3.5
$\text{CBr}_3\text{COCBr}_3$	334 ^b	- ^b	- ^b	- ^b	290	-
$\text{CBr}_3\text{CONH}_2$	300	-	277	2.5^c	258	-
CBr_3F	306	0.8	289	0.7	257	0.5
$\text{C}_3\text{Br}_2\text{F}_6$	278	~ 0.5	252	~ 0.3	<230	-
CBr_3H	294	~ 0.4	275	~ 0.3	245	~ 0.1
CBr_4	338	1.5	315 ^d	0.8 ^d	275	1.0

- a) In CH_2Cl_2 at 20°C . b) Complex formation was followed by (more or less fast) irreversible chemical reaction (see the Experimental Section for details) which hindered measurements of formation constants. c) Interaction of $\text{CBr}_3\text{CONH}_2$ with NCS^- may involve hydrogen bonding (vide infra). d) From ref. 15.

On the whole, the formation constants, K , of the complexes with pseudohalides are in the same range as those measured earlier for the analogous R-Br molecules with bromide anions.[10] The highest values of K were observed in the systems with the strong electrophiles, such as CBr_3CN or CBr_3NO_2 , and the lowest constants were measured with CHBr_3 or $\text{C}_3\text{Br}_2\text{F}_6$. Most importantly, the graph in Figure 2 demonstrates a clear correlation between the energies of the electronic transition in the $[\text{R-Br}, \text{A}^-]$ complexes and the difference of the energies of the lowest unoccupied molecular orbitals ($E_{\text{LUMO}}^{\text{R-Br}}$) of the R-Br electrophile and the highest occupied molecular orbitals ($E_{\text{HOMO}}^{\text{A}}$) of the pseudohalide. This Mulliken correlation includes the absorption bands of complexes with pseudohalides and previously reported[10] halogen-bonded associates with bromide anions.

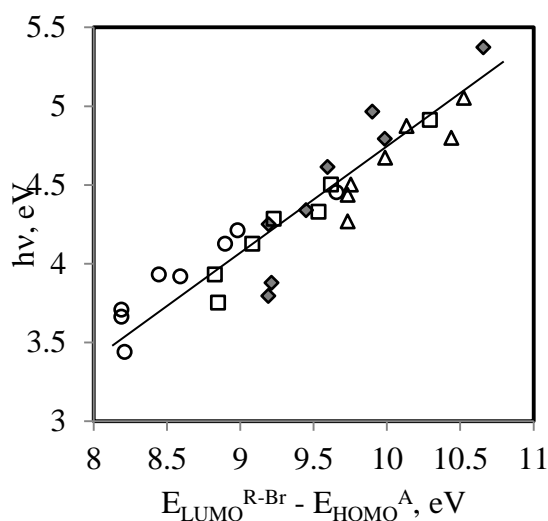


Figure 2. Mulliken correlation between the energies ($h\nu$) of the (lowest-energy) absorption bands of $[\text{R-Br}, \text{A}^-]$ complexes and the difference of the frontier orbital energies ($E_{\text{LUMO}}^{\text{R-Br}} - E_{\text{HOMO}}^{\text{A}}$) of the interacting species for the R-Br associates with N_3^- (\circ), NCS^- (\square), NCO^- (\triangle), and Br^- (\diamond) anions (see Table S1 in the Supporting Information for details).

The intense absorption bands in the UV-Vis spectra of the $[\text{R-Br}, \text{A}^-]$ complexes and the Mulliken correlation of their energies point out that orbital (charge-transfer) interaction plays a significant role in the formation of these associates. [24,25] To determine structural features of

the intermolecular bonding in these systems, we turn to the X-ray crystallographic and computational analysis of the R-Br/A⁻ associates.

2. Crystallization and X-ray structural characterization of the solid-state associates.

Co-crystals of the bromocarbons with the pseudohalides were obtained via the diffusion of hexane into dichloromethane solutions containing an R-Br electrophile from Chart I and tetrapropylammonium salts of cyanate, thiocyanate, or azide anion (see the Experimental Section for the details). For example, diffusion of hexane into a dichloromethane solution containing equimolar amounts of CBr₃NO₂ and (Pr₄N)NCO⁻ resulted in the formation of colorless crystalline materials. FT-IR-spectra of the resulting materials show characteristic absorption bands of the CBr₃NO₂ electrophile together with those of Pr₄N⁺ cation and NCO⁻ anion (see Figure S6 in the Supporting Information). Similar crystalline materials showing IR absorption bands of R-Br electrophiles, pseudohalide anions and tetrapropylammonium cations (which appeared as the most suitable counter-ion for these crystallizations) were obtained in the solutions containing CBr₄/NCO⁻, CBr₄/NCS⁻, CBr₄/N₃⁻, and CBr₃CONH₂/NCS⁻ mixtures (see Table S2 in the Supporting Information).

(Pr₄N)NCO·CBr₃NO₂, (Pr₄N)NCO·CBr₄, (Pr₄N)N₃·CBr₄. X-ray crystallographic measurements established that (isostructural) crystals formed in solutions containing (Pr₄N)NCO salt and CBr₃NO₂ or CBr₄, as well as analogous (Pr₄N)N₃/CBr₄ pair of reagents are characterized by monoclinic unit cells (space group P2₁/n). They comprised anions and bromocarbons in a 1:1 ratio, with each electrophile being coordinated (via its three bromine substituents) with three anions, and in turn, each anion being coordinated with three bromocarbon molecules. Such 3:3 coordinations lead to the formation of zigzag layers (Figure 3 and Figure S7 in the Supporting Information) which are separated by Pr₄N⁺ counterions.

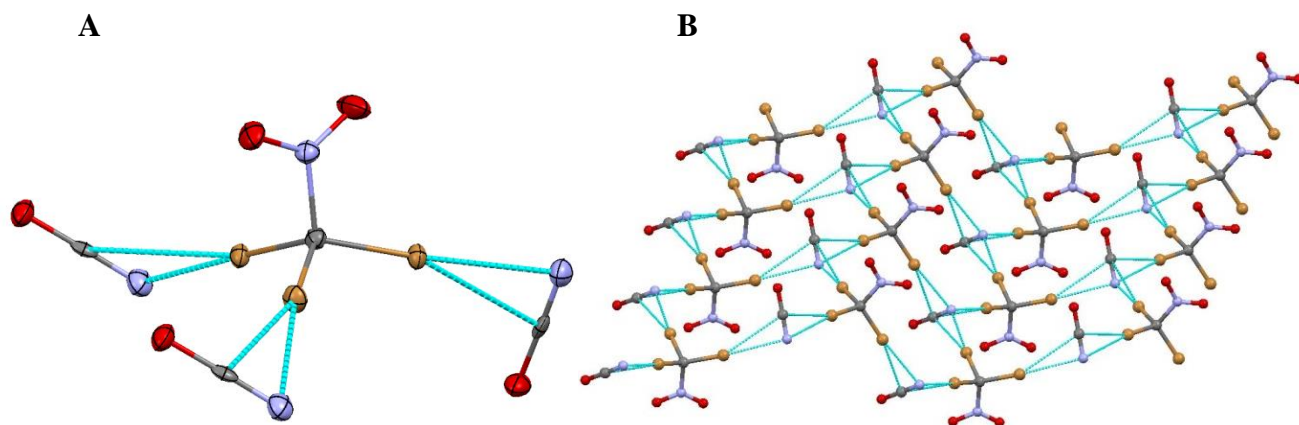


Figure 3. (A) Fragment of the X-ray structure of the $(\text{Pr}_4\text{N})\text{NCO}\cdot\text{CBr}_3\text{NO}_2$ co-crystals illustrating short contacts (blue lines) between tribromonitromethane and cyanate anion. (B) Zigzag layer formed by (3:3) coordination of tribromonitromethane and NCO^- anions (for clarity, Pr_4N^+ cations are not shown).

The R-Br/ NCO^- and R-Br/ N_3^- layers consist of uniform chair-like cells resembling distorted cyclohexane molecules in which C-C bonds are replaced with C-Br... NCO^- (or C-Br... N_3^-) fragments. In most cases, the C-Br bonds of the electrophile are directed toward C-N (or N-N) bonds of the pseudohalide. As a result, the bromine atoms of R-Br molecules show close contacts with the terminal and central atoms of the neighboring anions (Figure 3A). For example, in the co-crystal formed by CBr_3NO_2 with NCO^- , the intermolecular Br...N distances are 2.763 Å, 3.004 Å, and 3.212 Å (Table 2). The corresponding distances to central carbon atoms of the same anions are longer (3.370 Å, 3.291 Å and 3.222Å, see Table S3 in the Supporting Information), but they are still less than the corresponding sum of the van der Waals radii (3.55 Å [26]). In all three structures, the increase of the distances between bromine and the terminal atom of the anion is accompanied by the decrease of the distance to the corresponding central atom of the pseudohalide (Table S3 in the Supporting Information).

Table 2. Halogen bond geometries in the [R-Br, A⁻] co-crystals.^a

Co-crystals	Contact	D(Z-X...Y), Å	∠(Z-X...Y), deg	∠X-X...Br), deg	R _{XY}
(Pr ₄ N)N ₃ ·CBr ₄	Br3...N1	2.875(3)	167.66(12)	99.3(2)	0.85
	Br2...N1	2.806(3)	176.90(11)	108.2(2)	0.83
	Br4...N1	3.216(4)	160.48(18)	79.0(2)	0.95
(Pr ₄ N)NCO·CBr ₄	Br2...N1	2.823(3)	176.39(12)	109.7(3)	0.83
	Br4...N1	2.937(3)	167.40(12)	96.5(2)	0.86
	Br3...N1	3.188(3)	173.74(12)	79.8(2)	0.94
(Pr ₄ N)NCO·CBr ₃ NO ₂	Br2...N3	3.004(3)	167.74(9)	94.4(2)	0.88
	Br1...N3	2.763(3)	176.06(9)	112.9(2)	0.81
	Br3...N3	3.212(3)	173.50(9)	80.3(2)	0.94
2((Pr ₄ N)NCS)·CBr ₄	Br4...S1	3.2309(11)	171.76(11)	93.23(13)	0.92
	Br1...S1	3.2147(11)	170.15(11)	108.83(13)	0.91
	Br3...N1	3.013(3)	167.07(13)	139.2(3)	0.89
	Br2...N2	2.897(4)	172.74(13)	136.5(3)	0.85
2((Pr ₄ N)NCS)·CBr ₃ CONH ₂	Br2...S2	3.2294(6)	174.50(6)	96.21(8)	0.88
	Br3...S1	3.3377(6)	178.02(6)	79.13(8)	0.91
	Br1...S1	3.5286(6)	151.85(7)	123.56(8)	0.95

^{a)} See Table S3 in the Supporting Information for the atom labeling and characteristics of the other short intermolecular contacts in these co-crystals. b) $R_{XY} = D_{X...Y}/(r_X + r_Y)$, where $D_{X...Y}$ is the intermolecular separation between X and Y, and r_X and r_Y are their van der Waals radii, i.e. 1.85 Å for bromine, 1.55 Å for nitrogen and 1.80 Å for sulfur.[26]

The C-Br...N angles (where N is a terminal nitrogen atom of azide or cyanate anion) are in the typical for halogen bonding range of 167–177° (Table 2). In comparison, the C≡N...Br (or N=N...Br) angles are within the 79–115° range, i.e. halogen bonds in these systems are almost orthogonal to the main axes of the pseudohalide molecules. Such intermolecular distances

and angles suggest that halogen bonds in these systems involve predominantly π -bonds of the pseudohalide anions, similar to that observed earlier with metal-coordinated cyanide ligands.[13]

Scrutiny of the intramolecular geometries of the azide anion (Table S4 in the Supporting Information) showed that the halogen bonding of one its ends with three CBr_4 molecules results in significant alteration of the intra-azide bonds. Specifically, the bond length of the $\text{N}=\text{N}$ fragment involved in halogen bonding of $1.121(4)$ Å is about 8% shorter than the bond length of the non-bonded end of azide anion of $1.210(4)$ Å. Similar contraction of the bond involved in intermolecular interactions was related earlier to the fact that charge transfer from this bond is overcompensated by the charge shift from the other side of the pseudohalide.[23] The intramolecular NCO^- bonds in the co-crystals of cyanate with carbon tetrabromide ($\text{C}\equiv\text{N}$ bond of $1.145(5)$ Å and $\text{C}-\text{O}$ bond of $1.245(4)$ Å) are rather close to the corresponding values in the co-crystals with tribromonitromethane ($\text{C}\equiv\text{N}$ bond of $1.136(3)$ Å and $\text{C}-\text{O}$ bond of $1.239(3)$ Å) [While the cyanate and thiocyanate anions can be presented as a resonance between several Lewis structures, e.g. $\text{N}\equiv\text{C}-\text{O}^-$ and $^-\text{N}=\text{C}=\text{O}$, carbon-nitrogen bonds of these anions will be shown hereinafter as a triple bond, and their carbon-oxygen and carbon-sulfur bonds will be shown as a single bond, for clarity.]

$2((\text{Pr}_4\text{N})\text{NCS})\cdot\text{CBr}_4$. Co-crystallization of $(\text{Pr}_4\text{N})\text{NCS}$ with carbon tetrabromide produced colorless needle-like crystals containing thiocyanate and $\text{R}-\text{Br}$ electrophiles in a 2:1 ratio. They comprise zigzag ladders formed by 3:3 coordination of NCS^- anions and CBr_4 molecules. Each carbon tetrabromide also coordinates an additional (exterior) thiocyanate via a halogen bond involving its fourth bromine substituent and the nitrogen atom of the NCS^- anion (Figure 4). These halogen-bonded networks are separated by Pr_4N^+ counterions.

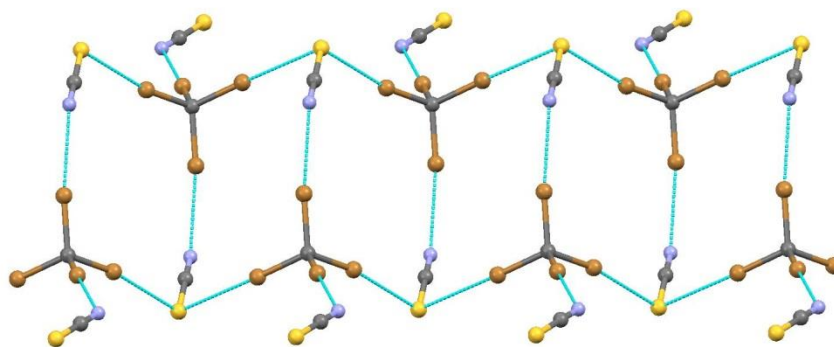


Figure 4. Zigzag ladders formed by (3:3) coordination of carbon tetrabromides and thiocyanate anions, with the additional (exterior) pseudohalides coordinated to the remaining bromine substituents of R-Br electrophile (for clarity, Pr_4N^+ cations are not shown).

Within the network, each thiocyanate anion links two CBr_4 molecules via two nearly perpendicular halogen bonds involving its sulfur atom. Nitrogen atoms of these NCS^- anions form terminal halogen bonds with a third carbon tetrabromide. In turn, each CBr_4 molecule is halogen-bonded to three (intra-network) NCS^- anions and to one exterior pseudohalide (Figure 4). The $\text{Br}\dots\text{S}$ and $\text{Br}\dots\text{N}$ halogen bonding results in a similar contraction (8 to 10 %) of the $\text{Br}\dots\text{S}$ and $\text{Br}\dots\text{N}$ distances as compared to the sum of their van der Waals radii, and all $\text{C}\dots\text{S}$ and $\text{C}\dots\text{N}$ angles in this structure are about 170° (Table 1). On the other hand, the $\text{C}\dots\text{S}\dots\text{Br}$ angles (93° and 109°) are noticeably lower than the $\text{C}\equiv\text{N}\dots\text{Br}$ angles of about 138° .

$2((\text{Pr}_4\text{N})\text{NCS})\cdot\text{CBr}_3\text{CONH}_2$. Co-crystallization of $(\text{Pr}_4\text{N})\text{NCS}$ with tribromoacetamide produced colorless plates with 2:1 $(\text{Pr}_4\text{N})\text{NCS}:\text{CBr}_3\text{CONH}_2$ stoichiometry. Similar to the $((\text{Pr}_4\text{N})\text{NCS})\cdot\text{CBr}_4$ co-crystals, they comprise zigzag ladders formed by 3:3 electrophile/anion bonding, with each $\text{CBr}_3\text{CONH}_2$ molecule binding an additional (exterior) thiocyanate (Figure 5).

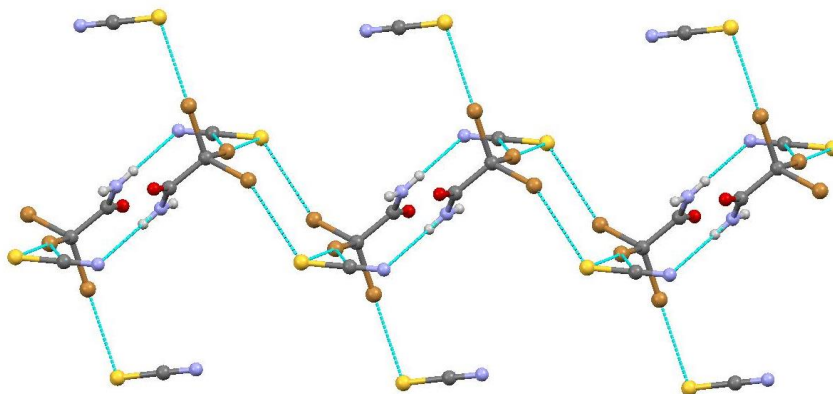


Figure 5. Zigzag ladders formed by halogen and hydrogen bonds between tribromoacetamide and thiocyanate anions (showing as blue lines), with the additional (exterior) pseudohalides halogen-bonded to the remaining bromine substituents of R-Br electrophile (for clarity, Pr_4N^+ cations are not shown).

In this structure, each tribromoacetamide molecule forms three $\text{Br}\dots\text{S}$ halogen bonds with two intra-network anions and one exterior thiocyanate, and its amide group is hydrogen-bonded with the nitrogen atom of a fourth (intra-network) pseudohalide anion. In turn, each intra-network thiocyanate shows three intermolecular bonds: its sulfur atom links two $\text{CBr}_3\text{CONH}_2$ molecules, and its nitrogen atoms form hydrogen bonds with amide groups of the third tribromoacetamide. The exterior thiocyanates are halogen-bonded with tribromoacetamide molecules via their sulfur atoms. The terminal $\text{Br}_2\dots\text{S}_2$ bond with exterior thiocyanate (which is involved only in one halogen bond) is somewhat shorter than the analogous bridging halogen bonds (Table 2). Regardless of the mode of intermolecular interaction, the C-N bonds of thiocyanate anions are around 1.16 Å, and their C-S bonds are close to 1.65 Å (see Table S4 in the Supporting Information).

3. Computational characterization of the [R-Br, A⁻] complexes.

The geometry of [R-Br, A⁻] adducts were fully optimized via DFT computations with M06-2X functional in combination with 6-311+G(dp) basis set (see the Experimental Section for the details). For most of the R-Br/A⁻ pairs, these computations afforded multiple local energy minima and equilibrium geometries of adducts. In particular, all R-Br molecules showed two modes of halogen bonding with cyanate and thiocyanate anions (Figures 6), i.e. C-Br...N-C and C-Br...X-C (where X= O or S). The calculations of the complexes of CBr₃CONH₂ with thiocyanate also produced adducts formed via hydrogen bonding as well as a combination of halogen and hydrogen bonds between the electrophile and pseudohalide illustrated in Figure 6F.

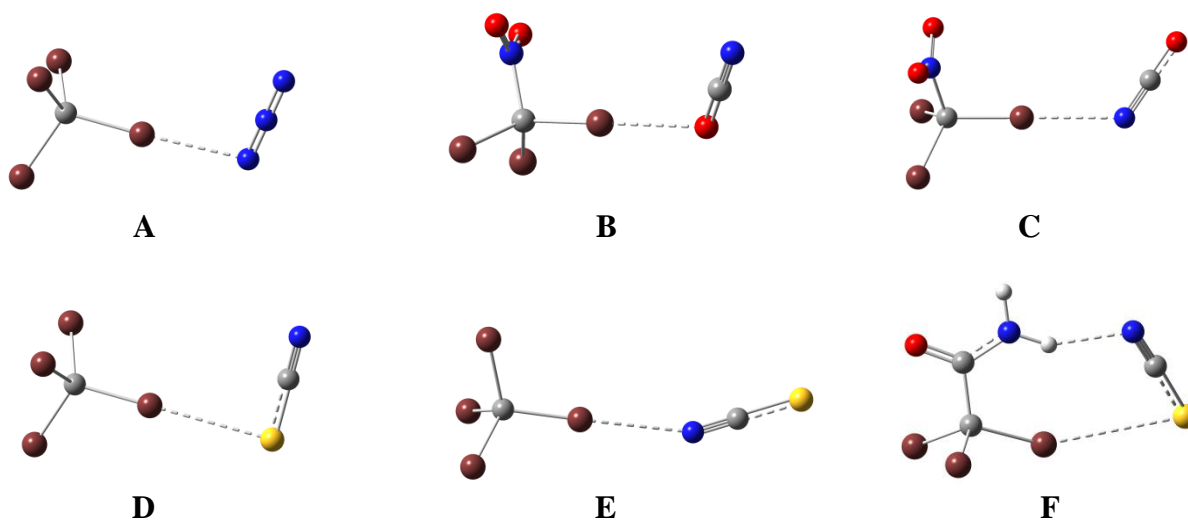


Figure 6. Principal modes of halogen-bonding in R-Br/A⁻ pairs resulted from the M06-2X/6-311+G(dp) computations (see Experimental Section for details).

The calculated interaction energies and geometric characteristics of some of the R-Br/A⁻ adducts formed via different modes of halogen bonding in the gas phase and in dichloromethane are listed in Table 3 and Table S5 in the Supporting Information.

Table 3. Interaction energies and principal geometric characteristics of the R-Br·A⁻ adducts. ^a

Adduct	Mode	ΔE , ^b kcal mol ⁻¹		$d_{\text{Br}\dots\text{X}}$, Å		$\angle\text{YXB}$, °	
		gas-phase	CH ₂ Cl ₂	gas-phase	CH ₂ Cl ₂	gas-phase	CH ₂ Cl ₂
CBr ₄ ·N ₃ ⁻	Br...N	-18.32	-4.64	2.370	2.708	109.2	103.8
CBr ₄ ·NCO ⁻	Br...N	-16.40	-3.74	2.426	2.752	128.0	131.4
	Br...O	-13.21	-3.12	2.506	2.744	120.8	113.2
CBr ₃ NO ₂ ·NCO ⁻	Br...N	-20.99	-5.32	2.336	2.677	124.4	123.6
	Br...O	-16.39	-4.19	2.4563	2.689	120.3	118.9
CBr ₄ ·NCS ⁻	Br...S	-12.19	-3.13	2.865	3.187	98.1	92.4
	Br...N	-11.20	-2.62	2.616	2.842	158.1	157.1
CBr ₃ CONH ₂ ·NCS ⁻	Br...S	c	-2.08	c	3.295	c	85.2
	Br...N	c	-1.84	c	2.971	c	100.6
	Br...S/H...N	-20.95	-6.86	3.44	3.54	68.5	67.4
	Br...N/H...S	-19.12	-6.39	3.12	3.52	81.6	74.9

a) For the lowest energy minima representing various mode of halogen bonding which were observed in X-ray structures of the corresponding R-Br·A⁻ pair. The relevant characteristics of the other R-Br·A⁻ adducts are listed in Tables S5 and S6 in the Supporting Information. b) $\Delta E = E_{\text{complex}} - [E_{\text{R-Br}} + E_{\text{Br}}] + \text{BSSE}$, where E_{complex} , $E_{\text{R-Br}}$ and E_{Br} are sums of the electronic and zero-point energies, and BSSE is a basis set superposition error, see Experimental section. c) Computations produced only adducts showing combination of halogen and hydrogen bonding (see text).

In general, the binding energies, ΔE , between bromosubstituted electrophiles and pseudo-halide anions resulted from the M06-2X calculations in dichloromethane are in the same range (i.e. from -2 to -6 kcal/mol) as those obtained earlier for the analogous adducts with the bromide anion (in agreement with similar formation constants of complexes measured in solutions, *vide supra*).^[10] As expected for interactions involving charged species, the halogen bonding of R-Br

molecules and pseudohalides in the gas phase is stronger than in dichloromethane, and the differences of the corresponding values of ΔE in these two media are about 10 – 15 kcal/mol.

In complexes with cyanate anions, halogen bonding via the nitrogen end of the pseudohalide, C-Br...N \equiv C, is preferable over that involving the oxygen end. The differences of interaction energies between the corresponding adducts showing these two modes vary from 1 kcal/mol in CH₂Cl₂ to 4 kcal/mol in the gas phase. In comparison, the adducts bonded via sulfur atoms of thiocyanate are more stable than the adducts in which the bromine substituent of the same bromocarbons is attracted to the nitrogen end of the NCS⁻ anion. However, the differences of binding energies of these two modes are rather small (0.3 – 1.0 kcal/mol). Such minor distinctions are consistent with the experimental structural data, which revealed both modes of interaction in some of R-Br/NCS⁻ co-crystals (e.g., (Pr₄N)NCS)·CBr₄ reported herein), while only C-Br...S-C bonding was observed in the reported previously structure of (Bu₄N)NCS·CBr₄ [15] and in the co-crystals of thiocyanate anions with tribromoacetamide presented herein.

The lowest-energy CBr₃CONH₂/NCS⁻ adduct resulted from the DFT calculations shows a combination of halogen and hydrogen bonds (Figure 6F). In this adduct, the bromine substituent of CBr₃CONH₂ is halogen-bonded with the sulfur end of the thiocyanate and its amide group is hydrogen-bonded to the nitrogen end of the pseudohalide anion. The energy of the adduct showing the alternative, Br...N/H...S, combination of the halogen and hydrogen bonds is higher by 0.5 kcal/mol in CH₂Cl₂ and by 2 kcal/mol in the gas phase (Table 3). In comparison, the energies of the local minima for the CBr₃CONH₂/NCS⁻ pair in dichloromethane showing only halogen bonding (C-Br...S-C or C-Br...N \equiv C) are about 4 kcal/mol higher than those supported also by hydrogen bonds. In the gas phase, the optimizations of the CBr₃CONH₂/NCS⁻ pair led only to adducts stabilized by combination of halogen and hydrogen bonding analogous to those

in Figure 6F regardless of the starting geometry, and the equilibrium structure showing only halogen bonds with tribromoacetamide and thiocyanate were not found.

In accord with the binding energies, the adducts resulted from the calculations in the gas phase are characterized by the shorter intermolecular distances than the corresponding complexes in dichloromethane. Also, comparison of the results of calculations in Tables 3 with the X-ray structural data in Table 1 indicates that the Br...X separations calculated in the gas phase are also about 0.4-0.5 Å shorter than the corresponding experimental (solid-state) values. In fact, the latter are quite close to distances calculated in dichloromethane (the deviations are in the same range as the variations of the crystallographically independent separations measured for the same pair). A similar relationship between the experimental (X-ray structural) and calculated data was observed earlier for the halogen-bonded complexes between R-Br electrophiles and bromide anions.[10] It suggests that, at least for the computational method used herein, the adducts resulting from the calculations in moderately-polar dichloromethane represent a more realistic model of the experimental solid-state structures, in which R-Br/A⁻ interactions are significantly modulated by inter-ionic forces. We should note, however, that in the co-crystals, pseudohalide anions are bonded, in most cases, with several electrophiles and vice versa, which hinders comparison of the measured solid-state separations with the calculated interatomic distances in the 1:1 R-Br/A⁻ adducts in Table 3 (see the Experimental section for details). As such, more detailed theoretical study is required to establish relationship between the results of calculations in the gas-phase and in solution and the corresponding (solid-state) X-ray structures.

The relative orientation of the electrophile and pseudohalide moieties in the R-Br/A⁻ adducts resulting from the calculations in dichloromethane are similar to that found in the gas phase. Specifically, all halogen-bonded adducts are characterized by nearly linear C-Br...X

angles (where X = S, N or O). On the other hand, the angles between the main axis of the anion and halogen bond vary with the pseudohalide and the mode of interaction. Specifically, the N-N...Br angle in the $\text{CBr}_4/\text{N}_3^-$ adduct of about 104° (in CH_2Cl_2) and 109° (in the gas phase) are in the same range as the angles measured in the solid-state structure. In the adducts of CBr_4 or CBr_3NO_2 with cyanate anion halogen-bonded via the nitrogen atom, all C-N...Br angles are in $123 - 131^\circ$ range, i.e. they are somewhat higher than the corresponding experimental values. The analogous adducts bonded via oxygen atoms showed the C-O...Br angles in the $113-121^\circ$ range. In the thiocyanate adducts formed via C-Br...S-C halogen bond, the C-S...Br angles are close to 90° , in general agreement with the X-ray structural data. The $\text{C}\equiv\text{N}\dots\text{Br}$ angles in the corresponding associates halogen-bonded via nitrogen ends are about 138° in the solid-state co-crystals and about 157° in the calculated adducts. The complexes of thiocyanate with the iodoperfluorobenzenes obtained earlier similar distinctions between C-S...I and $\text{C}\equiv\text{N}\dots\text{I}$ angles, although adducts bonded via nitrogen were slightly more stable, possibly due the fact that they were carried out with different, B3LYP, functional.[16]

Comparison of the experimental and calculated data showed that relative orientations of the halogen-bonded R-Br electrophiles and pseudohalides which are observed in the X-ray structures are, on the whole, similar to those resulted from DFT (M06-2X /6-311+G(dp)) computations. Accordingly, they provide valuable information about the factors which determine the geometry of halogen bonding.

Indeed, halogen bonding is most commonly related to the electrostatic attraction between a positively charged area on the surface of the covalently-bonded halogen atom and a negative area on the surface of the electron rich nucleophile.[27, 28] Yet, experimental and computational data point out that weakly-covalent molecular orbital (or charge-transfer) interactions also play a

significant role in formation of many halogen-bonded complexes.[10, 15, 29] To elucidate this dichotomy for R-Br complexes with pseudohalides, we scrutinized the structures of their adducts vis a vis surface electrostatic potentials (ESP) of the interacting species (critical for electrostatic interactions) and frontier orbital shapes (involved in the orbital interactions).

Up to now, the structural studies of halogen bonding were focused mostly on the properties of the halogen-bond donors and on the linear C-X...Y angles (which are observed in the majority of halogen-bonded complexes where X is an halogen and Y is a nucleophile). [6,10,27,28] However, for the halogen-substituted electrophiles, in particular CBr_4 , CBr_3NO_2 and $\text{CBr}_3\text{CONH}_2$ (Figure 7), the positive potential on the surface of halogen atoms, as well as major fractions of their LUMOs are located along the extension of the C-Br bonds. Accordingly, both the electrostatic model (which relies on the attraction of the areas of opposite electrostatic potentials) and the molecular-orbital approach (which requires effective HOMO/LUMO overlap) predict that the contacts of halogenated electrophiles with halogen bond acceptors should be located near the extension of the C-Br bond and essentially linear C-Br...X angle.

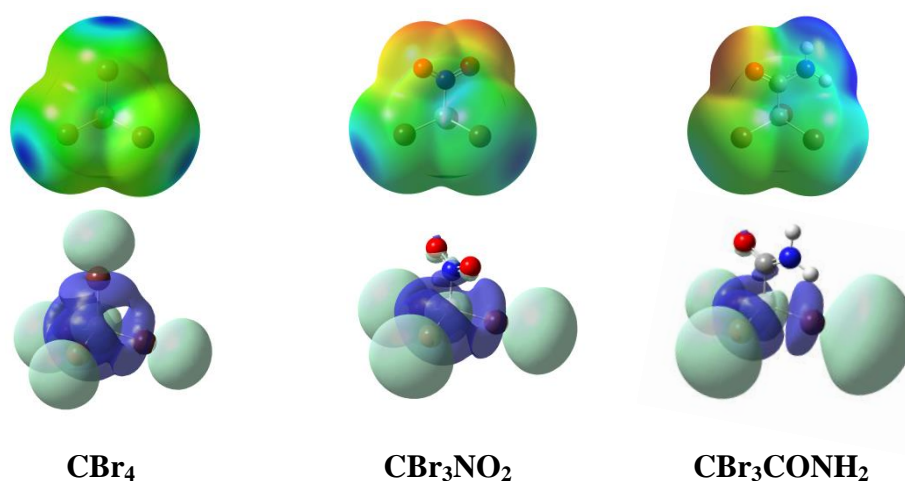


Figure 7. Surface electrostatic potentials (top) and LUMO shapes (bottom) of R-Br electrophiles (as indicated) resulted from MP2/6-311+G(dp) computations (see Experimental Section for the details). Blue and red colors in the top figures depict areas of positive and negative ESPs on the molecular surfaces of electrophiles, respectively, light and dark blue colors in the bottom figures depict opposite wavefunction phases.

On the other hand, the examination of the ESP and frontier orbital shapes of the azide, cyanate and thiocyanate anions revealed differences in the locations of the area of the maximum electrostatic potential and the major HOMO fragments for these pseudohalides. Specifically, the anionic N_3^- , NCO^- and NCS^- species are characterized by negative potentials over all their surfaces. Yet, the scrutiny of the ESP values in a narrower range revealed that the areas of the most negative electrostatic potential on the surfaces of all pseudohalides anions are located on the top of the nitrogen ends, i.e. along the extension of $\text{C}\equiv\text{N}$ bonds in OCN^- and SCN^- anions and $\text{N}=\text{N}$ bond in N_3^- anion (Figure 8). On the other hand, the major fragments of HOMOs are located in areas perpendicular to the terminal atoms.

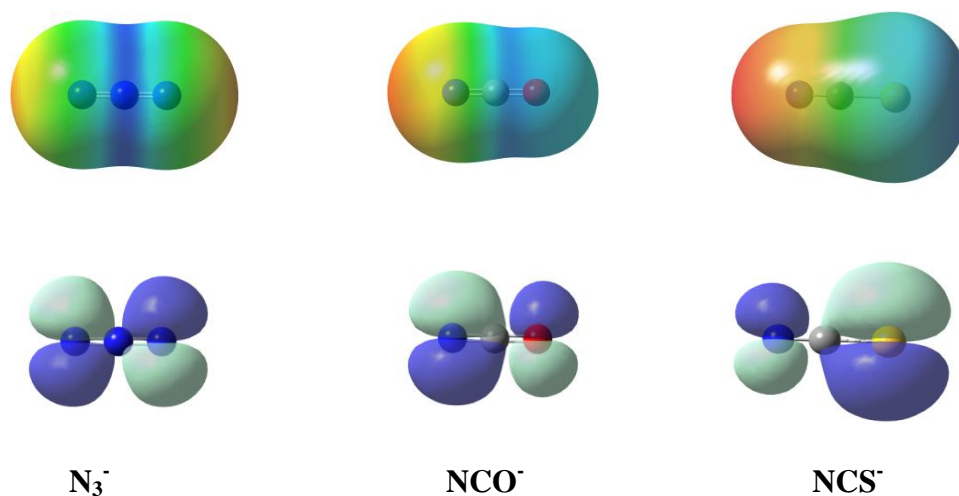


Figure 8. Surface electrostatic potentials (top) and HOMO shapes (bottom) of pseudohalide anions resulted from MP2/6-311+G(dp) computations (see Experimental Section for the details). Light and dark blue colors in the bottom figures depict opposite wavefunction phases. The ESP in the top figures are shown in the narrow ranges of negative potentials, i.e. for N_3^- : from -0.210 (red) to -0.185 (blue), for NCO^- : -0.237 (red) to -0.180 (blue), and for NCS^- : -0.253 (red) to -0.110 (blue, ESP potentials are in hartrees).

Thus, based on the electrostatic model, the anion/electrophile contacts in their halogen-bonded adducts are expected to be located preferably at the top of the nitrogen end of the pseudohalide, and the structures of the most stable complexes would show close to linear X-

N...Br angle. Yet, neither experimental X-ray (solid-state) structures nor calculated adducts agree with this prediction. In comparison, superposition of the MO shapes onto the X-ray (or calculated) structures of the halogen-bonded associates clearly indicate that intermolecular R-Br/A⁻ contact involves in all cases significant, if not maximum, HOMO/LUMO overlap (Figure 9). The locations of the contacts are also consistent with the results of the earlier analyses of intermolecular bonding with participation of azide and thiocyanate anions based on the electron localization function,[16, 22] since the latter largely follows molecular orbital picture. Furthermore, a similar relation between the location of the intermolecular contacts on the surface of the halogen-bond acceptor (as opposed to the highest ESP areas) was observed earlier in the halogen-bonded complexes of carbon tetrabromide with bromometallate anions.[7a] This suggests that molecular orbital interactions play a definitive role in the relative arrangements and intermolecular contacts of halogen bond donors and acceptors in their supramolecular complexes.

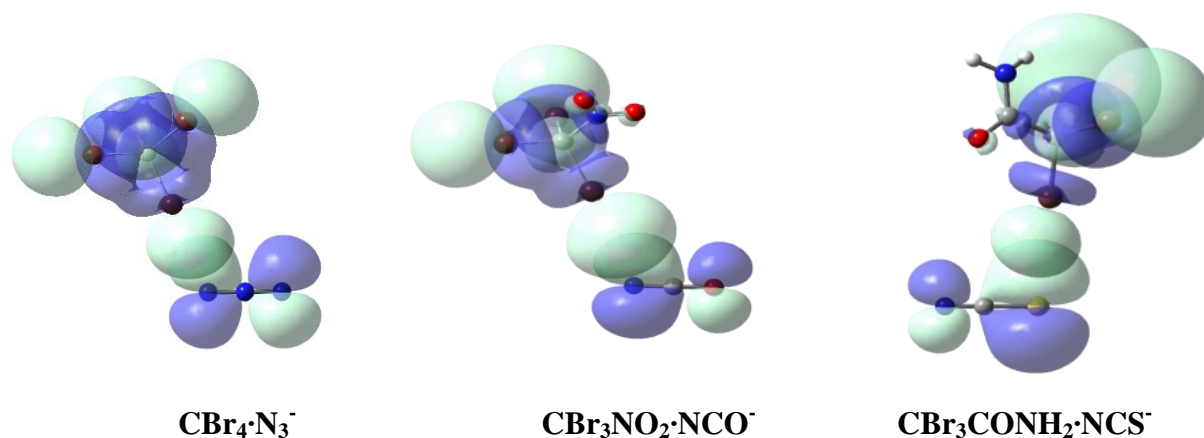


Figure 9. Frontier (HOMO/LUMO) orbital shapes of pseudohalide anions and R-Br electrophiles superimposed onto fragments of the crystal structures of their complexes

To evaluate the charge transfer resulting from such HOMO/LUMO interactions and its effect on the intramolecular and intermolecular geometries, we carried out Natural Bond Orbital

(NBO) analysis of the halogen-bonded complexes. The amount of charge, Δq , transferred from the pseudohalide to the electrophile in halogen-bonded $R-Br/A^-$ adduct is determined by the energy difference and overlap of the LUMO of the $R-Br$ electrophile and the HOMO of the pseudohalide.[30] Its value varies from $0.028e$ calculated for the adduct of bromoform with cyanate in dichloromethane to $0.316e$ for the adducts of the tribromonitromethane with azide in the gas phase (see Table S6 in the Supporting Information). The NBO calculations indicated that this charge is transferred mostly to the C-Br antibonding orbital, $\sigma^*(C-Br)$. It suggests that charge transfer should be accompanied by the elongation of the C-Br bonds in the electrophiles. Indeed, the plot in Figure 10 demonstrates clear correlation between the calculated amount of charge transfer, Δq , and the elongation of the C-Br bonds of bromocarbons, Δd .

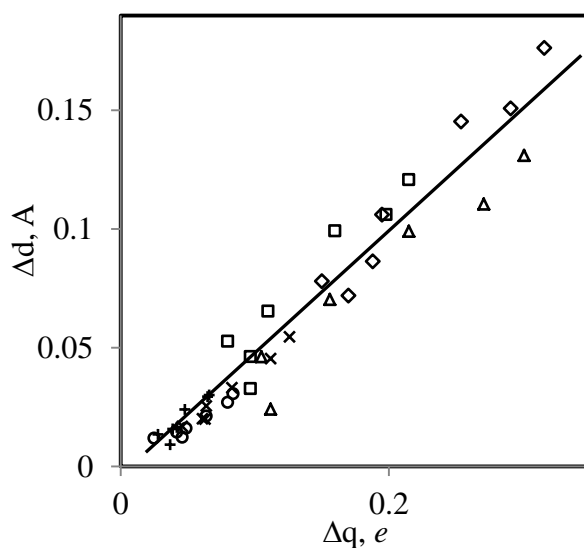


Figure 10. Relationship between calculated values of charge transfer in the $R-Br \cdot A^-$ adducts, Δq , and lengthening of the C-Br bonds, Δd (where Δd is a sum of the differences between C-Br bond lengths in the halogen-bonded and isolated $R-Br$ molecule) in the gas phase: $R-Br \cdot N_3^-$ (\diamond), $R-Br \cdot NCO^-$ (\square), $R-Br \cdot NCS^-$ (\triangle), and in solution: $R-Br \cdot N_3^-$ (\times), $R-Br \cdot NCO^-$ ($+$), $R-Br \cdot NCS^-$ (\circ), see Table S7 in the Supporting Information for the details).

Furthermore, the average C-Br bond length in the halogen bonded complexes of carbon tetrabromide with azide (1.951 Å), cyanate (1.949 Å) and thiocyanate (1.948 Å) obtained from the X-ray structural measurements are consistently higher than that of the separate CBr₄ molecule (1.930 Å [8b]). (The relatively small variations of C-Br bond length in the crystal structures of the halogen-bonded complexes together with limited number of such structures, differences in bonding modes and crystal-force effects precluded the use of experimental data for quantitative analysis of the correlation between Δd and Δq). Similar increase of the average bond length was observed earlier in the complexes of various bromocarbons with bromide anions.[10] The elongation of the C-Br bonds confirms that Δq values result not just from more or less arguable assignment of the charges to various atoms, but also are clearly manifested in the structural features of the interacting species.

The ratio of intermolecular distances between the interacting species to their van der Waals separations, $R_{XY} = D_{X...Y}/(r_X + r_Y)$, (where $D_{X...Y}$ is the intermolecular separation between X and Y, and r_X and r_Y are their van der Waals radii) also shows definitive correlation with the amount of the $A^- \rightarrow R-Br$ charge transfer (Figure 11). Noticeably, different pseudohalides show nearly parallel trends. The complexes of thiocyanate demonstrated the largest decrease of the intermolecular Br...S distances (i.e., at the same value of Δq , their R_{XY} are the lowest). In the complexes with cyanate, the intermolecular separations are less sensitive to charge transfer. Most importantly, the plots corresponding to various anions are characterized by correlation coefficients of 0.99. Since R_{XY} represents the structural manifestation of the strength of the intermolecular interactions, such correlations also strongly imply that HOMO/LUMO interactions and charge transfer play a significant role in halogen bonding between bromocarbons and pseudohalides.[30]

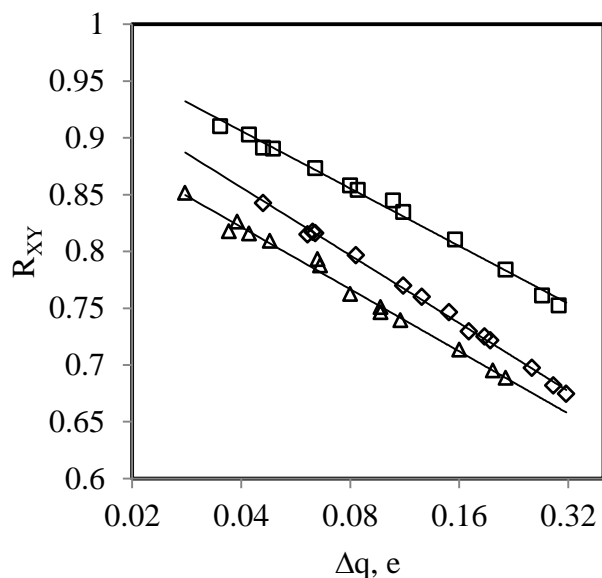


Figure 11. Correlation between charge-transfer, Δq , and ratio R_{XY} of the intermolecular distances in $R\text{-Br}\cdot A^-$ adducts to the corresponding van der Waals separations for $R\text{-Br}\cdot N_3^-$ (\diamond), $R\text{-Br}\cdot NCO^-$ (\square) and $R\text{-Br}\cdot NCS^-$ (Δ), see Table S6 in the Supporting Information for the details.

Taken together, Figures 10 and 11 demonstrate that, as the amount of charge transfer is rising, the intermolecular distance between interacting species is decreasing and C-Br bond lengths is increasing. As a result, the intermolecular Br...N bond of 2.29 Å in the $CBR_3NO_2\cdot N_3^-$ adduct calculated in the gas phase is comparable to the adjacent intramolecular C-Br bond length of 2.08 Å. It suggests that the electron is essentially delocalized between interacting species in the C-Br...N fragment, and that such bonding becomes similar to the (basically covalent) three-center four-electron model suggested for the description of the bonding in the trihalide anions.[31]

Conclusions.

The experimental and computational results presented in the current work demonstrate that pseudohalides form halogen-bonded associates with bromosubstituted electrophiles in the solid

state and in solution comparable in strength to those involving halide anions. The basic geometric characteristics of these associates established herein provide a background for the use of halogen bonding with pseudohalides for the molecular recognition of these anions and crystal engineering of their solid-state materials. The works in these directions look especially promising in view of the polydentate nature of the pseudohalides, which implies the possibility of multicenter interaction involving N_3^- , NCO^- and NCS^- anions via combination of halogen and hydrogen or coordination bonding.

Spectral and structural features of the halogen-bonded complexes with pseudohalides (in particular, the geometry of halogen bonding at the halogen-bond acceptor side) indicated that molecular orbital (charge-transfer) interactions play a significant role in their formation. Two implications of this conclusion should be underscored. First, the increase of the contribution of the charge-transfer interactions provides continuous transition from the weak complexes (in which it might be essentially neglected) to the strongly-bonded adducts in which intermolecular interactions approach a (more or less) conventional covalent bond. Second, as was shown earlier for the π -bonded complexes, orbital interactions attenuate barriers for electron transfer between the interacting species and, if electronic coupling is strong, leads to complete electron delocalization.[32] In a similar way, orbital interactions may dramatically reduce barriers for electron transfer between halogen-bond donors and acceptors.[33] In fact, our preliminary analysis indicated that the interaction between the strongest R-Br electrophiles (e.g. CBr_3NO_2) and N_3^- or NCS^- anions results in the irreversible electron transfer process, and the rate constants of these reactions may be accounted only if electronic coupling between halogen-bonded redox centers is taken into account. It point out that halogen bonding affect reactivity of halogenated molecules in solutions and conducting properties of their solid-state materials.

Experimental Section.

Commercially available bromoform, tribromofluoromethane, carbon tetrabromide, hexabromoacetone, and 1,2-dibromohexafluoropropane were purified by sublimation or distillation under vacuo. Tribromonitromethane was synthesized by bromination of nitromethane, tribromoacetamide was prepared by reaction of hexabromoacetone with NH_4OH , and tribromoacetonitrile was synthesized by dehydration of tribromoacetamide with P_2O_5 , as described earlier.[34] Commercially available tetrabutylammonium salts of azide, cyanate and thiocyanate anions were purified by recrystallization. Pseudohalide salts with the tetrapropylammonium counter-ions were prepared according to the procedures described in the literature by reaction of NaN_3 with $(\text{Pr}_4\text{N})\text{Cl}$, KNCO with $(\text{Pr}_4\text{N})\text{BF}_4$ and KNCS with $(\text{Pr}_4\text{N})\text{Br}$. [35]

The details of the UV-Vis measurements and the calculations of the formation constants of the $[\text{R}-\text{Br}, \text{A}^-]$ complexes were described previously.[10] It should be noted that while the complexes of CBr_3NO_2 , CBr_3CN or $\text{CBr}_3\text{COCBr}_3$ with NCO^- anions were persistent, absorption bands of the same electrophiles with NCS^- or N_3^- anions decreased with time, which indicated that irreversible chemical processes were occurring in these systems. They apparently involve dissociative electron transfer reactions proceeding via halogen-bonded complexes (as described earlier for the systems involving carbon tetrabromide or tribromonitromethane and tetramethyl-p-phenylenediamine [33]) and their kinetics and mechanism will be presented separately. To minimize effects of the irreversible processes, spectral measurements in the current work were carried out immediately after mixing.

Single crystals of halogen-bonded associates suitable for X-ray measurements were obtained by diffusion of hexane into dichloromethane solutions containing a 1:1 molar ratio of the R-Br bromocarbon from Scheme 1 and a pseudohalide (taken as a salt with tetrapropylammonium counter-ion) in CH_2Cl_2 at -20°C . For example, the tetra-n-propylammonium cyanate

salt (27 mg, 0.10 mmol) was dissolved together with tribromonitromethane (10 μ L, 0.10 mmol) in CH_2Cl_2 (2 mL) in a Schlenk tube. The resulting solution was carefully layered with of a 1:1 CH_2Cl_2 / hexane mixture (\sim 1 mL), and then with hexane (20 mL), and kept at -35°C . Slow diffusion of hexane into the dichloromethane resulted in the formation of colorless crystals suitable for single-crystal X-ray crystallography. FT-IR spectra of these crystals (recorded using single-reflection HATR) demonstrated strong absorption bands of tribromonitromethane (shifted as compared to the bands of the isolated CBr_3NO_2 molecule), alkylammonium cation, and cyanate anion (see Figure S6 in the Supporting Information). Single crystals $(\text{Pr}_4\text{N})\text{N}_3\cdot\text{CBr}_4$, $(\text{Pr}_4\text{N})\text{NCO}\cdot\text{CBr}_4$, $2((\text{Pr}_4\text{N})\text{NCS})\cdot\text{CBr}_4$, and $2((\text{Pr}_4\text{N})\text{NCS})\cdot\text{CBr}_4\cdot\text{CONH}_2$, were obtained and characterized in a similar way.

Single crystals suitable for X-ray diffraction studies were mounted using oil on a glass fiber. All measurements were made on a APEX-II CCD using Mo $\text{K}\alpha$ radiation ($\lambda = 0.71073 \text{ \AA}$) at 100(2) K. The structures were solved by direct methods and refined by full matrix least-squares treatment, and intermolecular contacts were analyzed using OLEX2 structure solution, refinement and analysis program.[36] CCDC 988299 - 988303 contain the supplementary crystallographic data for this paper. These data can be obtained free of charge from the Cambridge Crystallographic Data Centre via www.ccdc.cam.ac.uk/data_request/cif.

$(\text{Pr}_4\text{N})\text{NCO}\cdot\text{CBr}_4$. $\text{C}_{14}\text{H}_{28}\text{N}_2\text{OBr}_4$, $M = 560.02$, monoclinic, $a = 8.3579(5) \text{ \AA}$, $b = 19.0038(11) \text{ \AA}$, $c = 12.9329(7) \text{ \AA}$, $\beta = 98.504(2)^\circ$, $V = 2031.6(2) \text{ \AA}^3$, $T = 100.01$, space group $\text{P}2_1/\text{n}$ (no. 14), $Z = 4$, $\mu(\text{CuK}\alpha) = 9.673$, 18884 reflections measured, 3412 unique ($R_{\text{int}} = 0.0310$) which were used in all calculations. The final $wR(F_2)$ was 0.0723 (all data). CCDC 988300.

$(\text{Pr}_4\text{N})\text{NCO}\cdot\text{CBr}_3\text{NO}_2$. $\text{C}_{14}\text{H}_{28}\text{N}_3\text{O}_3\text{Br}_3$, $M = 526.12$, monoclinic, $a = 8.3003(4) \text{ \AA}$, $b = 18.9573(10) \text{ \AA}$, $c = 12.9480(6) \text{ \AA}$, $\beta = 98.635(2)^\circ$, $U = 2014.29(17) \text{ \AA}^3$, $T = 100.0$, space group

$P2_1/n$ (no. 14), $Z = 4$, $\mu(\text{MoK}\alpha) = 6.024$, 100523 reflections measured, 6198 unique ($R_{\text{int}} = 0.0439$) which were used in all calculations. The final $wR(F_2)$ was 0.0488 (all data). CCDC 988302.

$(Pr_4N)N_3 \cdot CBr_4$. $C_{13}H_{28}N_4Br_4$, $M = 560.03$, monoclinic, $a = 8.3581(7) \text{ \AA}$, $b = 19.1124(17) \text{ \AA}$, $c = 12.8700(11) \text{ \AA}$, $\beta = 98.448(2)^\circ$, $U = 2033.6(3) \text{ \AA}^3$, $T = 102.58$, space group $P2_1/n$ (no. 14), $Z = 4$, $\mu(\text{MO K}\alpha) = 7.916$, 115435 reflections measured, 5978 unique ($R_{\text{int}} = 0.0795$) which were used in all calculations. The final $wR(F_2)$ was 0.0811 (all data). CCDC 988299.

$2((Pr_4N)NCS) \cdot CBr_4$, $C_{27}H_{56}Br_4N_4S_2$, $M = 820.52$, monoclinic, $a = 7.8335(5) \text{ \AA}$, $b = 36.215(2) \text{ \AA}$, $c = 12.8318(8) \text{ \AA}$, $\beta = 91.767(3)^\circ$, $U = 3638.6(4) \text{ \AA}^3$, $T = 99.95$, space group $P2_1/n$ (no. 14), $Z = 4$, $\mu(\text{MoK}\alpha) = 4.561$, 103018 reflections measured, 10754 unique ($R_{\text{int}} = 0.1852$) which were used in all calculations. The final $wR(F_2)$ was 0.1002 (all data). CCDC 988301.

$2((Pr_4N)NCS) \cdot CBr_3CONH_2$. $C_{28}H_{58}Br_3N_5OS_2$, $M = 784.64$, monoclinic, $a = 10.0945(3) \text{ \AA}$, $b = 11.5019(4) \text{ \AA}$, $c = 31.8838(11) \text{ \AA}$, $\beta = 98.4293(13)^\circ$, $V = 3661.9(2) \text{ \AA}^3$, $T = 100.03$, space group $P2_1/n$ (no. 14), $Z = 4$, $\mu(\text{CuK}\alpha) = 5.359$, 19742 reflections measured, 6113 unique ($R_{\text{int}} = 0.0228$) which were used in all calculations. The final $wR(F_2)$ was 0.0759 (all data). CCDC 988302.

Computations. Quantum-mechanical calculations were carried out using the Gaussian 09 suite of programs.[37] Geometries of R-Br molecules, pseudohalide anions and [R-Br, Br⁻] complexes were optimized in the gas phase and in dichloromethane via DFT calculations with MO6-2X functional.[38] In our previous study of the halogen-bonded complexes between R-Br electrophiles and bromide anions, this method (as well as $\omega\text{B97X-D}/6\text{-311+G(dp)}$ computations) provided the best, on the whole, agreement between experimental and calculated (structural,

thermodynamic and spectral) characteristics of the intermolecular associates.[10] 6-311+G(d,p) basis set was employed in all computations. Results of the computations using ω B97X-D functional or *ab initio* MP2 method were consistent with the data obtained from the MO6-2X/6-311+G(d,p) calculations.

Geometry optimizations were carried out without constraints using the default convergence criteria for Gaussian 09 except in cases that required tighter convergence criteria to obtain true minima (as indicated by the absence of imaginary frequencies). Geometry optimizations in dichloromethane were carried out using polarizable continuum model (PCM).[39] The energies of interaction were determined by subtracting the sum of the energies of isolated R-Br and A⁻ species from the energy of the [R-Br, A⁻] complexes and adding basis set superposition error (BSSE): $\Delta E = E_{\text{complex}} - [E_{\text{R-Br}} + E_{\text{Br}}] + \text{BSSE}$, where E_{complex} , $E_{\text{R-Br}}$ and E_{Br} are sums of the electronic and zero-point energies.). The BSSE values for [R-Br, Br⁻] complexes were determined via the counterpoise method.[40] Zero-point energies (ZPE) and thermal corrections were taken from unscaled vibrational frequencies. Energies and atomic coordinates of halogen-bonded R-Br·Br⁻ associates are listed in the Supporting Information. Note, that calculations of the R-Br/A⁻ pairs produced, in most cases, multiple local minima. Some of these local minima showed rather minor differences in geometry (e.g. different torsion angles between the main axis of anion and carbon bond to non-halogen-bonded substituent in electrophile, such as C-N...C-N angle in the CBr₃NO₂/NCO⁻ associate) and in energy (< 0.3 kcal/mol). In such cases, only characteristics of the lowest-energy minimum are presented. It is also important to stress that while calculated structures represent 1:1 adducts, the X-ray structural data results from the characterization of the co-crystals in which anions may be bonded with several bromocarbons (and vice versa). For example, in the X-ray structure of 2(Pr₄N)NCS·CBr₃CONH₂ co-crystal,

one of the crystallographically independent thiocyanate links three carbon tetrabromide molecules via hydrogen N...H bond and two S...Br halogen bonds. Another thiocyanate is halogen bonded with one CBr₄ molecule via S...Br halogen bond. Noticeably, the latter bond of 3.229 Å is shorter than the separations between bromines and the bridging sulfur of 3.338 Å and 3.529 Å (Table 1). Similarly, in the 2(Pr₄N)NCS·CBr₄ structure, intermolecular Br...N separation of 2.897 Å between carbon tetrabromide and thiocyanate involved in one halogen bond is about 0.1 Å shorter than the analogous distance to the nitrogen of the bridging thiocyanate which forms three halogen bonds. These distinctions should be taken into account when calculated structures are compared with the X-ray structures. For the current work, most important is consistency of the relative orientations of the halogen bond donors and acceptors in their adducts which were obtained from the computations in the gas-phase and in CH₂Cl₂ (despite the distinctions of the intermolecular separations), as well as observed in the solid-state structures involving R-Br molecules and anions forming multiple and single halogen bonds.

Atomic charges were calculated via Natural Population Analysis phase of NBO analysis implemented in the Gaussian 09 suite of program.[41] Frontier orbital shapes were evaluated at 0.02 isovalue and electrostatic potentials were calculated on the 0.0004 electrons bohr⁻³ molecular surfaces of the R-Br molecules and pseudohalide anions resulted from MP2/6-311+G(dp) computations.

Acknowledgements

We thank Alfredo Traversa and Eric Loboda for the assistance with synthesis of tetrapropylammonium salts of pseudohalides and some spectral measurements. We also thank National Science Foundation (grant CHE-1112126) for the financial support of this work.

References.

1. (a) P. Metrangolo and G. Resnati, *Cryst. Growth Des.*, 2012, **12**, 5835. (b) W.T. Pennington, G. Resnati and M. S. Taylor, *CrystEngComm*, 2013, **15**, 3057.
2. (a) P. Metrangolo, H. Neukirch, T. Pilati and G. Resnati, *Acc. Chem. Res.*, 2005, **38**, 386. (b) P. Metrangolo, F. Meyer, T. Pilati, G. Resnati and G. Terraneo, *Angew. Chem., Int. Ed.* 2008, **47**, 6114.
3. P. Metrangolo and G. Resnati, *Halogen Bonding: Fundamentals and Applications*, Springer, Berlin, 2008.
4. G. Cavallo, P. Metrangolo, T. Pilati, G. Resnati, M. Sansotera and G. Terraneo, *Chem. Soc. Rev.*, 2010, **39**, 3772.
5. (a) M. G. Sarwar, B. Dragisic, S. Sagoo and M.S. Taylor, *Angew. Chem., Int. Ed.*, 2010, **49**, 1674. (b) E. A. L. Gillis, M. Demireva, M. G. Sarwar, M.G. Chudzinski, M. S. Taylor, E. R. Williams and T.D. Fridgen, *Phys. Chem. Chem. Phys.*, 2013, **15**, 7638. (c) M.G. Sarwar, B. Dragisic, E. Dimitrijevic and M.S. Taylor, *Chem. - Eur. J.*, 2013, **19**, 2050. (d) A. Caballero, F. Zapata, N.G. White, P. J. Costa, V. Felix and P.D. Beer, *Angew. Chem., Int. Ed.*, 2012, **51**, 1876. (e) J. A. Vargas, D. Emery, J. Mareda, P. Metrangolo, G. Resnati and S. Matile, *Angew. Chem., Int. Ed.*, 2011, **50**, 11675. (f) F. Zapata, A. Caballero, N. G. White, T.D.W. Claridge, P. J. Costa, V. Felix and P.D. Beer, *J. Am. Chem. Soc.*, 2012, **134**, 11533. (g) M. Cametti, K. Raatikainen, P. Metrangolo, T. Pilati, G. Terraneo and G. Resnati, *Org. Biomol. Chem.*, 2012, **10**, 1329.
6. (a) L. Brammer, G.M. Espallargas and S. Libri, *CrystEngComm*, 2008, **10**, 1712. (b) F. Zordan, L. Brammer and P. Sherwood, *J. Am. Chem. Soc.*, 2005, **127**, 5979. (c) G. M. Espallargas, L. Brammer and P. Sherwood, *Angew. Chem., Int. Ed.* 2006, **45**, 435.
7. (a) S.V. Rosokha and M.K. Vinakos, *Cryst. Growth Des.*, 2012, **12**, 4149. (b) S. V. Rosokha, J. J. Lu, T.Y. Rosokha and J.K. Kochi, *Chem. Commun.*, 2007, 3383.

8. (a) A. Farina, S.V. Meille, M. T. Messina, P. Metrangolo, G. Resnati and G. Vecchio, *Angew. Chem., Int. Ed.* 1999, **38**, 2433. (b) S.V. Lindeman, J. Hecht and J.K. Kochi, *J. Am. Chem. Soc.*, 2003, **125**, 11597. (c) J. Lieffrig, O. Jeannin, M. Fourmigue, *J. Am. Chem. Soc.*, 2013, **135**, 6200.
9. (a) H. Wang, X.R. Zhao and W.J. Jin, *Phys. Chem. Chem. Phys.*, 2013, **15**, 4320. (b) Q.J. Shen and W.J. Jin, *Phys. Chem. Chem. Phys.*, 2011, **13**, 13721-13729. (b) R. Cabot and A.C. Hunter, *Chem. Commun.*, 2009, 2005.
10. S. V. Rosokha, C. L. Stern and J.T. Ritzert, *Chem.- Eur. J.* 2013, **19**, 8774.
11. (a) H. Bock and S. Holl, *Z. Naturforsch. B*, 2002, **57**, 835. (b) H. Bock and S. Holl, *Z. Naturforsch. B*, 2002, **57**, 713.
12. A. Abate, J. Marti-Rujas, P. Metrangolo, T. Pilati, G. Resnati and G. Terraneo, *Cryst. Growth Des.*, 2011, **11**, 4220.
13. J.E. Ormond-Prout, P. Smart and L. Brammer, *Cryst. Growth Des.*, 2012, **12**, 205.
14. R.D. Walsh, J.M. Smith, T. W. Hanks and W.T. Pennington, *Cryst. Growth Des.*, 2012, **12**, 2759.
15. (a) S.V. Rosokha, I.S. Neretin, T.Y. Rosokha, J. Hecht and J.K. Kochi, *Heteroat. Chem.*, 2006, **17**, 449. (b) S.V. Rosokha and J.K. Kochi, in *Halogen Bonding: Fundamentals and Applications*, ed. P. Metrangolo and G. Resnati, Springer, Berlin, 2008, pp. 137-160.
16. P. Cauliez, V. Polo, T. Roisnel, R. Llusar and M. Fourmigue, *CrystEngComm*, 2010, **12**, 558.
17. (a) J. Viger-Gravel, I. Korobkov and D.L. Bryce, *Cryst. Growth Des.*, 2011, **11**, 4984. (b) M. Formigue and P. Auban-Senzier, *Inorg. Chem.*, 2008, **47**, 9979.
18. CSD version 5.35 (November 2013). The search for the non-covalent intermolecular contacts shorter than sum of the corresponding van der Waals radii and involving covalently-bonded

chlorine, bromine or iodine atom and cyanate anions R-X...NCO or R-X...OCN (where X= Cl, Br, or I and R is Cl, Br, I or C) resulted in one structure (ref. code DOWXUI) in which Cl...O contact of 2.842Å is observed between copper-coordinated NCO⁻ anion and chloroform solvate. Similar search for the short contacts involving azide anions, R-X...N₃, resulted in 17 structures. However, all these structures involve contacts between metal-coordinated azide and halogen substituent of another ligand or chlorine from dichloromethane or chloroform solvate molecules (see Table S9 in the Supporting information for details).

19. (a) K. Bowman-James, A. Bianchi and E. Garcia-Espana, *Anion Coordination Chemistry*, Wiley VCH, Weinheim, 2011. (b) J. Ribas, A. Escuer, M. Monfort, R. Vicente, R. Cortes, L. Lezama and T. Rojo, *Coord. Chem. Rev.*, 1999, **193-195**, 1027. (c) W.P. Fehlhammer and W. Beck *Z. Anorg. Allg. Chem.*, 2013, **639**, 1053.
20. L. Tchertanov, *Supramol. Chem.*, 2000, **12**, 67.
21. (a) L. Tchertanov and C. Pascard, *Acta Crystallogr. B*, 1997, **B53**, 904. (b) L. Tchertanov and C. Pascard, *Acta Crystallogr. B*, 1996, **B52**, 685.
22. I.S. Bushmarinov, O.G. Nabiev, R.G. Kostyanovsky, M.Yu. Antipin and K.A. Lyssenko, *CrystEngComm*, 2011, **13**, 2930.
23. P. W. Schultz, G.E. Leroi and J.F. Harrison, *Mol. Phys.*, 1996, **88**, 217.
24. R.S. Mulliken and W. B. Person, *Molecular Complexes. A Lecture and Reprint Volume*, Wiley: New York, 1969.
25. E.V. Anslyn and D.A. Dougherty, *Modern Physical Organic Chemistry*, University Science Books, Sausalito, CA, 2006, p. 186.
26. A. Bondi, *J. Phys. Chem.*, 1964, **68**, 441.

27. (a) P. Politzer, J.S. Murray and T. Clark, *Phys. Chem. Chem. Phys.*, 2010, **12**, 7748. (b) P. Politzer, K. E. Riley, F.A. Bulat and J.S. Murray, *Comp. Theor. Chem.*, 2012, **998**, 2.
28. F. F. Awwadi, R. D. Willett, K. A. Peterson and B. Twamley, *Chem.- Eur. J.* 2006, **12**, 8952.
29. (a) J.-W. Zou, Y.-J. Jiang, M. Guo, G.-X. Hu, B. Zhang, H.-C. Liu and Q.-S. Yu, *Chem.- Eur. J.*, 2005, **11**, 740-51. (b) L.P. Wolters and F. M. Bickelhaupt, *ChemistryOpen*, 2012, **1**, 96. (c) X. An, B. Jing and Q. Li, *J. Phys. Chem. A*, 2010, **114**, 6438. (d) N.J. Martinez Amezaga, S. C. Pamies, N.M. Peruchena and G.L. Sosa, *J. Phys. Chem. A*, 2010, **114**, 552. (e) A. Yu. Rogachev and R. Hoffmann, *J. Am. Chem. Soc.*, 2013, **135**, 3262. (f) A. Yu. Rogachev and R. Hoffmann, *Inorg. Chem.*, 2013, **52**, 7161.
30. (a) Indeed, “ the major effect of the charge-transfer interaction is to allow the interacting molecules to move much closer to each other than would be possible if the interaction between molecules were purely electrostatic in nature”^{30b} (b) A.E. Reed, L. A. Curtiss and F. Weinhold, *Chem. Rev.*, 1988, **88**, 899.
31. G. A. Landrum, N. Goldberg and R. Hoffmann, *J. Chem. Soc., Dalton Trans.*, 1997, 3605.
32. S. V. Rosokha and J. K. Kochi, *Acc. Chem. Res.*, 2008, **41**, 641.
33. S. V. Rosokha and M. K. Vinakos, *Phys. Chem. Chem. Phys.*, 2014, 16, 1809.
34. (a) V. L. Heasley, D. R. Titterington, T. L. Rold and G. E. Heasley, *J. Org. Chem.*, 1976, **41**, 1285. (b) J.F. Arenas, J.I. Marcos and M.I. Suero, *An. Quin.*, 1984, **80**, 236. (c) M.I. Suero, L.I. McNeil and F. Marquez, *J. Raman Spectrosc.*, 1987, **18**, 273.
35. (a) H. Kobler, R. Munz, G.A. Gasser and G. Simchen, *Liebigs Ann. Chem.*, 1978, 1937. (b) I.K. Kukushkin, E.V. Velikanova and V. A. Zlobin, *Izv. Vys. Uch. Zav. Khim. Khim. Technol.*, 2010, **53**, 108.

36. (a) G.M. Sheldrick, SHELXTL Version 6.14; Bruker Analytical X-ray Instruments, Inc.: Madison, WI, 2003. (b) O.V. Dolomanov, L.J. Bourhis, R.J. Gildea, J.A.K. Howard and H J. Puschmann, *Appl. Cryst.*, 2009, **42**, 339.
37. Gaussian 09, Revision C.01, M. J. Frisch, G. W. Trucks, H. B. Schlegel, G. E. Scuseria, M. A. Robb, J. R. Cheeseman, G. Scalmani, V. Barone, B. Mennucci, G. A. Petersson, H. Nakatsuji, M. Caricato, X. Li, H. P. Hratchian, A. F. Izmaylov, J. Bloino, G. Zheng, J. L. Sonnenberg, M. Hada, M. Ehara, K. Toyota, R. Fukuda, J. Hasegawa, M. Ishida, T. Nakajima, Y. Honda, O. Kitao, H. Nakai, T. Vreven, J. A. Montgomery, Jr., J. E. Peralta, F. Ogliaro, M. Bearpark, J. J. Heyd, E. Brothers, K. N. Kudin, V. N. Staroverov, R. Kobayashi, J. Normand, K. Raghavachari, A. Rendell, J. C. Burant, S. S. Iyengar, J. Tomasi, M. Cossi, N. Rega, J. M. Millam, M. Klene, J. E. Knox, J. B. Cross, V. Bakken, C. Adamo, J. Jaramillo, R. Gomperts, R. E. Stratmann, O. Yazyev, A. J. Austin, R. Cammi, C. Pomelli, J. W. Ochterski, R. L. Martin, K. Morokuma, V. G. Zakrzewski, G. A. Voth, P. Salvador, J. J. Dannenberg, S. Dapprich, A. D. Daniels, O. Farkas, J. B. Foresman, J. V. Ortiz, J. Cioslowski, and D. J. Fox, Gaussian, Inc., Wallingford, CT, 2009.
38. Y. Zhao and D.G. Truhlar, *Theor. Chem. Acc.*, 2008, **120**, 215.
39. J.; Tomasi, B. Mennucci and R. Cammi, *Chem. Rev.*, 2005, **105**, 2999.
40. S. F. Boys and F. Bernardi, *Mol. Phys.*, 1970, **19**, 553.
41. (a) NBO Version 3.1, E. D. Glendening, A. E. Reed, J. E. Carpenter, and F. Weinhold. (b) F. Weinhold and C.R. Landis, *Discovering Chemistry with Natural Bond Orbitals*, Wiley, Hoboken, NJ, 2012.